Journal of Marine Research, 64, 517–540, 2006

The evolution of density currents and nepheloid bottom layers in the Ross Sea (Antarctica)

by Giorgio Budillon[1], Ettore Salusti[2] and Sergio Tucci[3]

ABSTRACT

In this study we have analyzed the thermohaline, light transmission and particulate matter data, obtained in the western sector of the Ross Sea during the *X* Italian Expedition, for the purpose of investigating the evolution of the High Salinity Shelf Water in this area. In particular CTD data were used to estimate the baroclinic velocity field. Light transmission and total particulate matter data (from Niskin bottles mounted on a Carousel water sampler) were used to analyze the nepheloid layers and the evolution of the suspended sediments. This basin is characterized by a northward flow of very dense High Salinity Shelf Water ($\theta \sim -1.95$°C, S $\sim$ 34.90), much colder than the incoming Circumpolar Deep Water ($\theta \sim 1.20$°C, S $\sim$ 34.70). We obtained a scenario in which the High Salinity Shelf Water interacts with the Circumpolar Deep Water along the Antarctic Slope Front, and deviates from its geostrophic equilibrium. Interestingly, this cold dense water mixes with Circumpolar Deep Water at the shelf break and flows downward until it seems to disappear. Below this cold flow, a thin turbulent current has been observed, again moving northward with a high velocity $\sim$ 0.2–1.0 m s^{-1}. This thin flow also contains high concentration of suspended matter produced by the interaction of the dense water and the bottom sediments. The various elementary mechanisms ruling the dynamics of such down-flows, namely the effects of topographic irregularities, bottom friction, Ekman benthic boundary layers or the effect of the variability of the Antarctic Circumpolar Current, which can push offshore the dense water, are discussed in this paper.

1. Introduction

The Southern Ocean is the only place in the world in which a current, the Antarctic Circumpolar Current (ACC), can flow around the globe unimpeded. The Southern Ocean is bounded by the Antarctic continent to the south, while the Subtropical Front is traditionally considered as its northern limit. The ACC carries the Circumpolar Deep Water (CDW), a voluminous water mass that extends down to a depth of $\sim$ 4000 m. The Ross Sea (Fig. 1) is one of the places in which the Antarctic Bottom Water is formed as a final result of the interaction of the Ross Sea shelf waters and the Circumpolar Deep Water, along the

1. Dipartimento di Scienze per l'Ambiente, Università degli Studi di Napoli Parthenope, Via Acton, 38, 80133 Naples, Italy. ***email: giorgio.budillon@uniparthenope.it***

2. INFN, Dipartimento di Fisica, Università degli Studi di Roma La Sapienza, P.le Aldo Moro 2, 00185 Rome, Italy.

3. Dipartimento per lo Studio del Territorio e delle sue Risorse, Università degli Studi di Genova, Corso Europa, 26, 16132 Genoa, Italy.

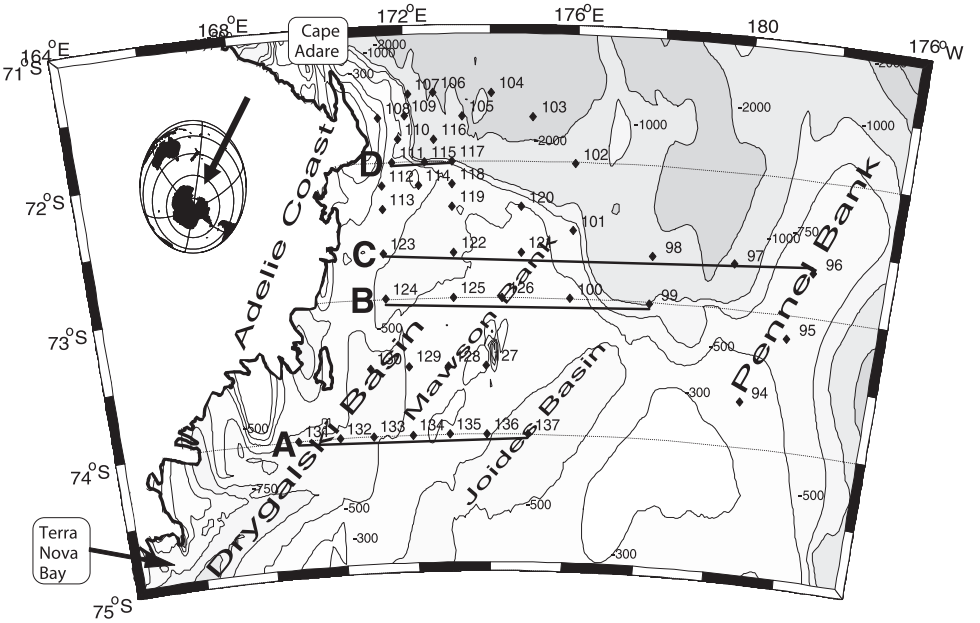

Figure 1. General map of the western Ross Sea with bottom topography (in meters), geographical position of the CTD stations and A-B-C-D transects.

Antarctic Slope Front. This CDW also reaches the Antarctic continental shelf break, where it is forced to mix with the shelf waters by the general circulation, giving rise to distinct water masses (Jacobs *et al.,* 1970; Gordon and Tchernia, 1972; Rodman and Gordon, 1982) such as the Antarctic Bottom Water (AABW). One of the most voluminous shelf waters is the very cold dense High Salinity Shelf Water (HSSW), easily detectable in the central-western sector of the Ross Sea. Moving northward, it reaches the continental shelf break and sinks toward the deepest oceanic layers where it takes part in the formation of the Antarctic Bottom Water. In this study dense shelf waters and their dynamics have been analyzed (Sections 1–4) in relation to the nepheloid layers. Indeed, in this region there is a relative abundance of sediments on the shelf and also a wealth of nepheloid layers. These come from moraine movements, catabatic winds, rock fragmentation due to the extreme environmental conditions and from other phenomena as well (Section 5).

Gordon *et al.* (2004) recorded the rapid descent of these dense shelf waters over the northern continental slope of the Ross Sea. The thickness of these currents was ~100–250 m and velocities up to 1.0 m s^{-1} were recorded, flowing at an angle of ~35° to the isobaths of the shelf-break. Of particular interest was a short-duration pulse of undiluted shelf water, that was observed at a depth of ~1400 m, moving at ~90° to the isobaths, with a remarkable speed of ~ 1.4–1.6 m s^{-1}.

Various elementary mechanisms can cause such down-flows. One has to consider either bottom currents that interact with some topographic irregularity (Wahlin and Walin, 2001;

Wahlin, 2004), bottom friction (Killworth, 2001), an Ekman benthic boundary layer (Baines and Condie, 1998) or the presence of the Antarctic Circumpolar Current which can push the slower moving dense water offshore. Furthermore, a current-bottom particulate interaction can also affect the evolution of density-turbidity currents (Smith, 1975; Hogg *et al.,* 2000; Necker *et al.,* 2002). In such a context, it is interesting to remember how Quadfasel *et al.* (1990) noted that in the Sulu Sea turbidity currents can bring relatively shallow clear waters to great depths. In summary, in this study we have analyzed the hydrological and sediment data sets to investigate the evolution of the HSSW in the Ross Sea, its sinking, mixing and final "disappearance" near the shelf break off Cape Adare, as well as its relationship with a thin benthic layer interacting with the sediments at the continental shelf break.

2. The Ross Sea

The Ross Sea is a continental sea on the Antarctic shelf in the Pacific sector of the Southern Ocean, between Cape Colbeck at 158W and Cape Adare at 170E (Fig. 1). A broad ice cover, the Ross Ice Shelf, extends over nearly half the continental shelf and is about 250 m thick on its northernmost side (Jacobs and Comiso, 1989). This only limits the uppermost waters, while deep waters can circulate freely under the floating ice shelf.

The sea-bottom of the central-western sector of the Ross Sea is characterized by alternating banks and basins, some of which are deeper than the platform edge. Indeed, the topography of the seafloor in this zone is irregular, with the ~500 m deep shelf isolated from the shore by a canyon more than 1000 m deep oriented north-eastward, the Drygalski Basin. Furthermore, the Ross Sea shelf is marked by a series of broad bathymetric troughs that run roughly northeast-southwest. These troughs were probably produced by glacial erosion during the last glacial period. A saddle ~100 m high lies at the shelf-edge end of the troughs and no major channel or canyon cut the shelf break, which lies at a depth of ~400–500 m (Davey and Jacobs, 2005). Off Cape Adare the shelf narrows northward; a rapidly deepening depression, the normal fault of Cape Adare, is located on the eastern side of the shelf.

The ACC moves around Antarctica, defining the northern limit of the Ross Sea. It carries the CDW ($\theta \sim 1.7$°C, $S \sim 34.72$) in its deepest layer. South of the ACC there are vast areas of clock-wise gyres: one of them is located north of the Ross Sea and extends between 160E and 140W. Off the Ross Sea shelf this CDW flows north-westward at velocities of 0.20–0.40 m s^{-1} (Gordon *et al.,* 2004). The mixing of the CDW with the surface and the shelf waters in the Ross Sea forms distinct water masses, such as the AABW ($\theta \sim -0.5$°C, $S \sim 34.70$) as described by Gordon (1967) and the Modified Circumpolar Deep Water (MCDW, with $\theta \sim -0.4$°C, $S \sim 34.52$; Budillon *et al.,* 2003). This is characterized by a subsurface potential temperature maximum and also a dissolved oxygen minimum (Jacobs *et al.,* 1985).

These shelf waters are formed during the Austral winter, when the upper layers cool and freeze, thus releasing part of their saline content (Jacobs *et al.,* 1985). Shelf waters

generally have temperatures close to the surface freezing point, between −1.95°C and −1.75°C and show higher salinity values in the western sector than in the eastern one (Locarnini, 1994). The densest of these waters are the HSSW ($\theta \sim -1.95$°C, S ∼ 34.90) formed along the western sector of the Ross Sea. They are known to move northward, following the clock-wise circulation (Budillon *et al.,* 1999, 2003).

A part of the HSSW, however, moves southward and flows under the Ross Ice Shelf (not shown on the map; Jacobs *et al.,* 1970) which is the southern boundary of the Ross Sea, forming a different type of cold water called Deep Ice Shelf Water, with an average salinity of 34.62. This cold water mass spreads over much of the shelf, where it occupies the deepest layer of the water column, between 400 m and the sea-bottom (Bergamasco *et al.,* 2002; Budillon *et al.,* 2002). Over this water mass, the Low Salinity Shelf Water (with $\theta \sim -1.73$°C, S ∼ 34.54) fills the intermediate to subsurface layers (Jacobs *et al.,* 1985; Budillon *et al.,* 2003).

The region where the shelf waters interact with the CDW has been identified as a narrow belt where thermohaline properties change abruptly, the Antarctic Slope Front. This important oceanographic feature of Antarctic shelf break zones is easily detectable by a temperature gradient of 2−3°C over 20−30 km (Jacobs, 1991). It is topographically controlled and, interestingly, has high biological productivity, being a source or sink region for heat, salt, nutrients, particulate, sediments and atmospheric gases (Trumbore *et al.,* 1991). It must be stressed that the presence of organic and inorganic particulate matter is significant and well distributed over the entire Ross Sea shelf.

3. Data collection and methodology

During the Austral summer 1994/1995 (January 7th to February 20th, 1995), the Italian CLIMA project carried out its first basin-scale oceanographic cruise in the northern Ross Sea and collected CTD casts (Fig. 1).

We first analyzed a subset of data relative to Cape Adare. The CTD casts were collected using a calibrated Sea Bird Electronics SBE 9/11 PLUS coupled to a Carousel water sampler SBE 32. The CTD was equipped with double temperature-conductivity sensors flushed at a constant rate. The calibration of temperature and conductivity sensors was performed at the SACLANT CENTER of La Spezia (Italy) before and after the cruise. During the cruise, the CTD temperature was checked with two SIS RTM4200 digital reversing platinum thermometers. Several samples of water were collected from different depths at every station, and analyzed on board, using an Autosal Guideline Salinometer. According to the pre-and-post cruise calibrations, an offset of −0.0028°C was applied to the raw temperature data.

Only the bottom samples were used for the salinometer corrections for the conductivity calibration. According to these data, an offset of 0.00095 S m^{-1} was applied to the raw conductivity data. The hydrological data were then corrected and processed according to international procedures (UNESCO, 1988). Standard algorithms (UNESCO, 1983) were used to compute quantities such as the potential temperature, salinity, potential density anomaly.

Sediment transport information came from light transmission measurements and direct concentration measurements. The light transmission measurements were made with a Seapoint Turbidity Meter sensor. This instrument measures scattered light (880 nm) at 15–150° to the axis of the beam from a small volume within 5 cm of the sensor windows. The sensitivity selected was 200 mV/FTU with a 25 FTU range. This sensor is factory adjusted for consistent responses to the Formazin Turbidity Standard measured in Formazin Turbidity Units (FTU). The Total Particulate Matter (TPM) concentration was determined during the cruise using a Seapoint sensor and water samples. The latter were collected during all seasonal cruises and filtered to measure the concentration and to calibrate the observed turbidity, with the TPM concentration in mg l^{-1}. The data are presented as light transmission (%). The depths at which water samples were collected were selected to coincide with selected layers of high optical turbidity (surface, intermediate and bottom nepheloid layers). Water samples were collected directly from the spigot of the Niskin bottle with a Teflon 10 liter vessel. A known sample volume between 2 and 3 liters was vacuum filtered (200 mm Hg) through a HA 47-mm diameter Millipore having a nominal pore size of 0.45 m and pre-weighed with a 10^{-5}g Scaltec SBC21 balance. After filtration the loaded membranes were rinsed with 60 ml Mill-Q water to remove sea salt. They were then air dried and stored in polystyrene Petri dishes at −20°C to await laboratory analysis. In the laboratory the filters were dried at 65°C for 3 hours using an ISCO stove and re-weighed to obtain the TPM concentration. Eventual variations due to varying atmospheric-environmental conditions were corrected using pre-weighed filters without samples for the correction (Pierce *et al.,* 1981); a control filter was used for every sampling station. Afterwards the filters were ashed for 3 hours with an ISCO muffle (ISM320 mod.) at 1100°C, using some acetone drops (Carlo Erba®) to remove the organic fraction. The unburned fraction was weighed and used as inorganic particulate fraction, as discussed by Piccazzo and Tucci (1983).

4. The measured fields

In this section we discuss the CTD data sampled along the Drygalski Basin where the HSSW flows northward. Using casts from 96 to 137 (sections A, B, C and D) we investigated processes occurring near the continental shelf break, where the CDW rises over the shelf interacting with the cold and salty shelf waters, modifying its properties and giving rise to the MCDW. In this sector of the Ross Sea the vertical structure of the water column is relatively simple, being formed by an Antarctic Surface Water layer of 50–70 m over the MCDW (when present) or the very cold HSSW, which occupies the water column near the seafloor. The MCDW layer is thicker close to the shelf break, while a massive presence of HSSW has been observed near its formation area (Terra Nova Bay, Fig. 1). Considering that the HSSW is almost isothermal ($\theta \approx -1.9$°C, the surface freezing temperature, and $S = 34.8$), while MCDW is characterized by a temperature greater than −0.8°C, the potential temperature θ finally represents a good tracer for analyzing the interactions between these water masses. The spreading of the HSSW over the shelf is

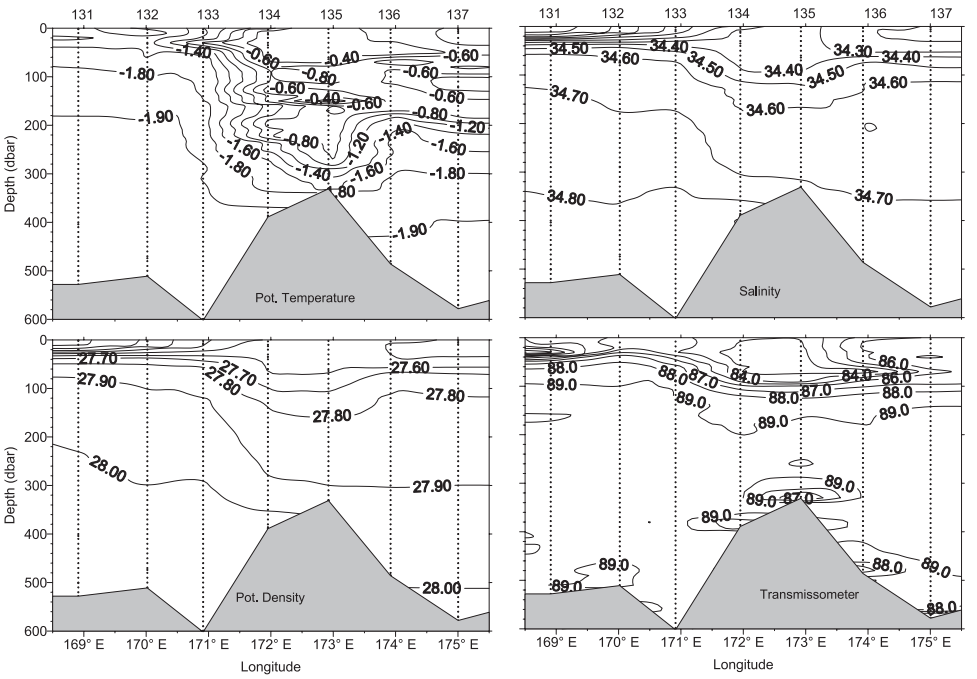

Figure 2. Vertical section of potential temperature (θ), salinity (S), and light transmission (%Tr) for transect A, identified by stations 131–137.

described here by vertical sections along zonal transects (Fig. 1) approximately perpendicular to the expected HSSW flow, with the northernmost transect being at the border of the shelf. In more detail:

a. Transect A—Stations 131–137 (14 February 1995, ~100 Nautical miles (Nm) long; Fig. 2)

A tongue of very dense cold HSSW is evident on the western side of this transect, between the Adelie Coast on the left and the Mawson Bank on the right. This layer is nearly isothermal ($\theta < -1.9$°C); the salinity is $S > 34.7$, increasing with the depth. This layer consists of HSSW formed in Terra Nova Bay. It flows northward toward the shelf break (roughly identified by the bathymetry of 500–1000 m, Fig. 1), following the bottom depression of the Drygalski Basin (Budillon *et al.,* 2000). Its velocity is ≈ 0.03 m s^{-1} greater than that of the upper layer, which is very slow as discussed later. This HSSW layer is ~ 300 m thick and the estimated HSSW flux is ~ 0.8 Sv. The Mawson Bank clearly separates the bottom layer which, on its eastern side, consists of shelf water of HSSW origin, already mixed with fresher shelf water (Budillon *et al.,* 2003).

Interestingly the light transmission data show a turbidity increase (corresponding to light transmission decrease of about 1–3% Tr) near the seafloor, particularly evident over the

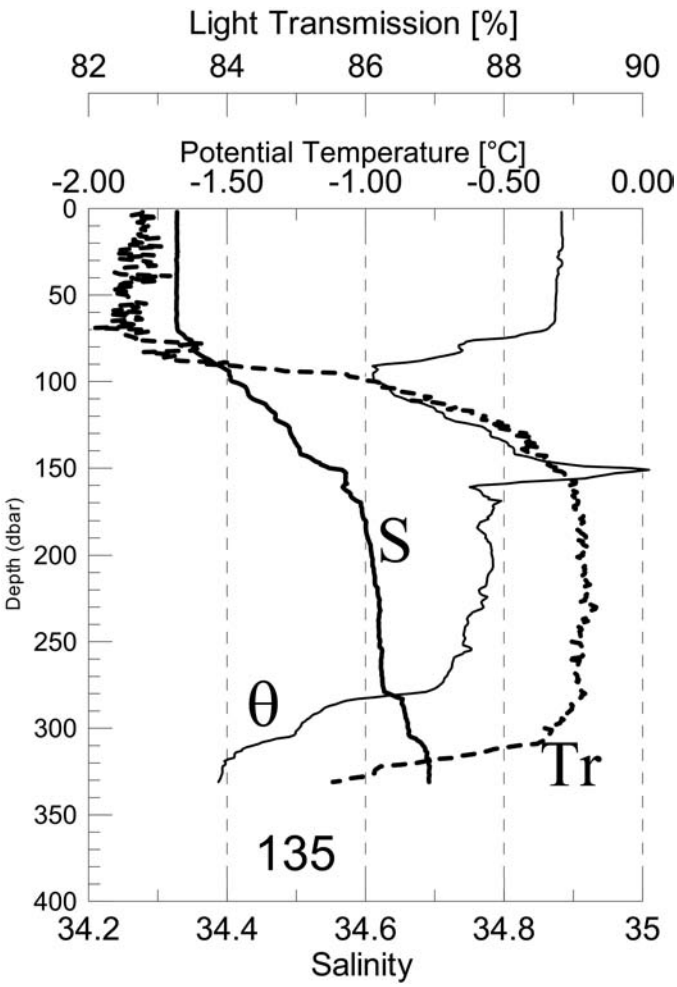

Figure 3. Potential temperature (θ), salinity (S), and light transmission (Tr) data versus depth for station 135, transect A.

Mawson Bank (stations 134, 135 and 136). This abrupt decrease in transparency is also evident in the CTD data of station 135 at ~ 50 m above the seafloor (Fig. 3, 280 m depth). A milder turbidity increase is also evident in the western part of this transect. The TPM data confirm such increases in turbidity, as an important benthic effect whose details are discussed in the following paragraphs.

b. Transect B—Stations 124-99 (8 February 1995, 116 Nm long; Fig. 4)

The HSSW is still present on the shelf on the western side of this transect, moving geostrophically (Smith, 1975; Wahlin and Walin, 2001) northward following the isobaths.

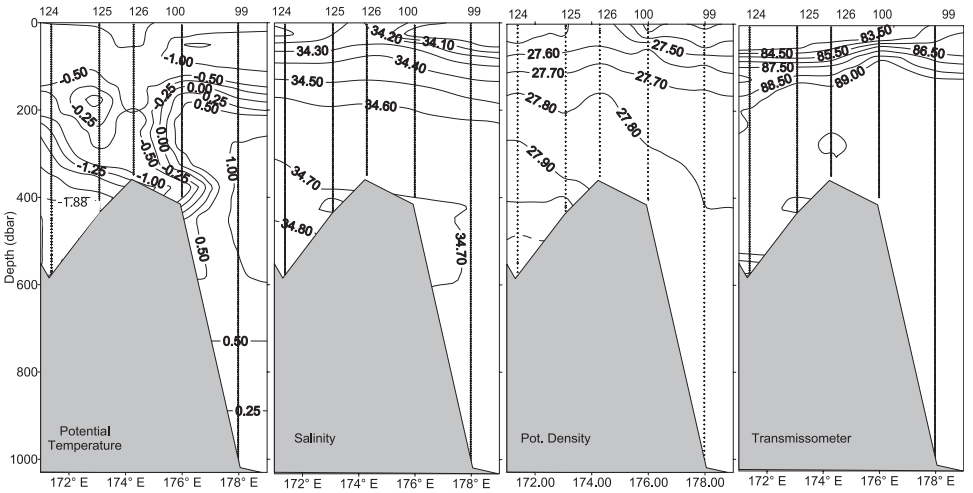

Figure 4. Vertical section of potential temperature (θ), salinity (S), and light transmission (%Tr) for transect B, identified by stations 124–99.

The potential density maximum is $\sigma_\theta = 28.06$, the bottom potential temperature and salinity are −1.88°C and 34.80 respectively, between stations 124 and 125. On the eastern side of this transect, between stations 126 and 99, the temperature near the bottom varies from −1.25°C at station 126, to +0.25°C at station 99. The salinity remains rather uniform, near to S ≅ 34.70. Again the HSSW velocity is ≈ 0.03 m s^{-1}, greater than the very low velocity of the upper layer. The HSSW layer is ∼ 250 m thick and the HSSW estimated flux is ∼ 0.4 Sv. The turbidity data show an abrupt decrease from surface water to a depth of 200 m (83.5 to 89.0% Tr), with a mild variation in the turbidity near the bottom. In this section the presence of a warm core of MCDW, flowing northwestward at an intermediate depth (∼400 m) but located east of the Mawson Bank, is particularly interesting. The strong horizontal gradients of salinity and potential temperature between HSSW and MCDW might be consistent with baroclinic instability processes, as remarked by one Referee.

c. Transect C—Stations 123-96 (6 February 1995, 180 Nm long; Fig. 5)

This section crosses the Drygalski Basin, the Mawson Bank, and the Joides Basin and finally touches the Pennel Bank, close to the eastern continental slope. The HSSW is still present on the western side of the shelf, flowing northward.

The most relevant feature of this section is, again, the longitudinal temperature gradient: at a depth of 300 m the temperature varies from −1.9°C, at station 123 to +1.30°C at station 98, where the deepest part of the offshore water column is occupied by MCDW. The salinity on the shelf varies between ∼34.64 at 200 m and the typical HSSW value ∼34.80 near the bottom. The potential density maximum is $\sigma_\theta = 28.0$ between stations

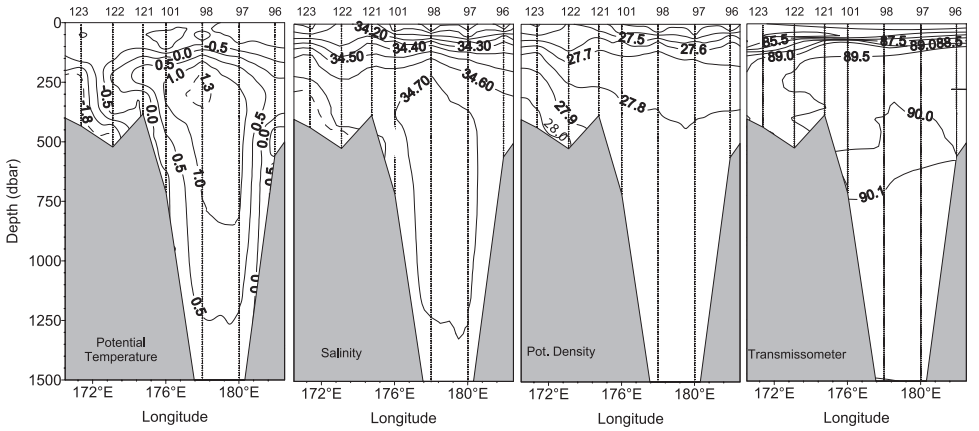

Figure 5. Vertical section of potential temperature (θ), salinity (S), and light transmission (%Tr) for transect C, identified by stations 123–96.

123 and 122. In this transect the slope of the isopycnal is really large, and of remarkable interest and shows a mild inversion between the surface level and the ~300–400 m level. This gives a baroclinic velocity between the sea surface and the bottom of ≈ 0.04 m s^{-1}, naturally correlated to the strong longitudinal temperature and salinity gradients in this area. The layer is ~20 m thick and the associated HSSW flux is ~ 0.3 Sv.

We observed that the light transmission casts had different behavior on the shelf and offshore. At a depth of 500 m, the western side of the section exhibited light transition values less than 89.5% while off the continental shelf the layer was characterized by values larger than 90.0% at the same depth.

d. Transect D—Stations 111-117 (11 February 1995, 26 Nm long; Fig. 6)

The shelf is narrow along this transect and interesting strong horizontal thermal and density gradients are evident. The HSSW completely disappears here while the maximum value of the density ($\sigma_\theta > 27.90$) at a depth of ~400 m underlines the presence of cold dense water ($\theta < -1.0$°C, $S > 34.70$), reminiscent of the HSSW (~80% HSSW and ~20% MCDW). This seems to flow as a "stream-tube" (Smith, 1975; Wahlin and Walin, 2001) toward the northwest. This "stream-tube" of shelf water has a velocity of ≈0.12 m s^{-1} relative to the adjacent strong current of MCDW moving toward the North-West, which appears to be pressing the tube to the bottom. The cold water core is ~130 m thick. The cold water core is ~130 m thick and the associated flux is ~0.2 Sv. The velocity of this MCDW has not been measured, but it usually ranges around 0.20 m s^{-1} (Gordon *et al.,* 2004).

The light transmission data did not show any significant signal correlated with this tube and the TPM concentration observed at station 111 was also somewhat surprising. Indeed, near the seafloor it was only ≈1.55 mg l^{-1} while at 200 m depths near the cold water it

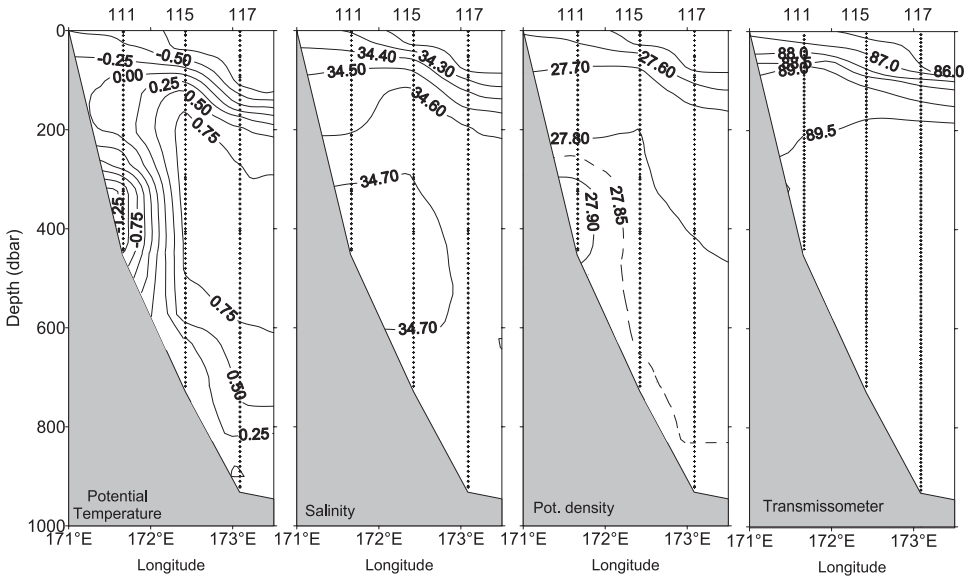

Figure 6. Vertical section of potential temperature (θ), salinity (S), and light transmission (%Tr) for transect D, identified by stations 111–117.

reached 3.24 mg l^{-1}. All this shows how resuspension phenomena were somewhat inhibited in the core of this cold water. Furthermore, when measuring the size and number of particles in the bottom water, we found a high number ($40-60 \times 10^6$ particles l^{-1}) of "small" inorganic particles (~1–3 μm) and a small number of "large" organic and inorganic particles (20–40 μm). The overall result was a mean size of $d \sim 3$ μm. The surrounding MCDW is, however, characterized by a lower number of heavier particles ($10-12 \times 10^6$ particles l^{-1}), with a mean size of $d \sim 30$ μm. In order to gain some insight into the composition of samples of casts 111 and 115, we carried out surveys using an electron microscope with microprobe and RX diffractometry. We found terrigenous particles (clay s.l., silicates of Ca, Fe and Mg) in the bottom nepheloid layer and an anomalous abundance of small fragments of biogenic origin (radiolaria, diatoms, frustules, sponge spicules). In the upper water column (MCDW) the amount of terrigenous matter was limited, but we found a great number of slightly fractured but still intact diatoms with strong traces of erosion. This supports the argument that the biogenic fraction present in MCDW has not been stressed mechanically against the sea bottom. Near the bottom the strong current of HSSW origin has enhanced the fracturing of the weak biogenic component of the suspended sediments until very small particulate was obtained, with slower re-sedimentation velocities.

In brief, the seafloor temperature on the Ross Sea shelf provides a good representation of the different areas occupied by the cold shelf waters and by the relatively warm MCDW, intruding over the shelf (Fig. 7). From the above data it is clear that the HSSW flows

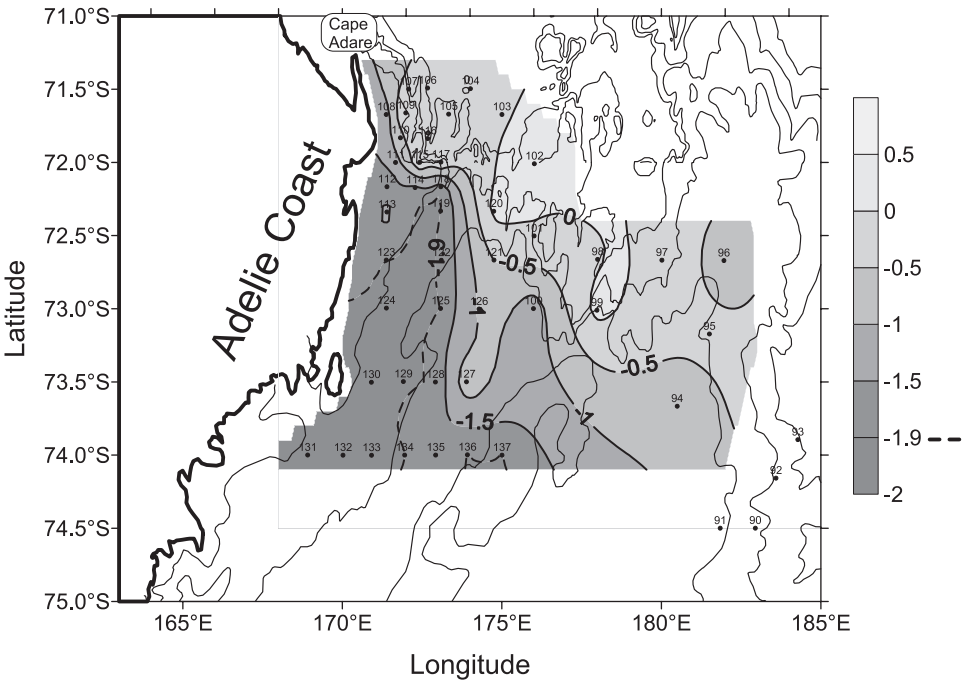

Figure 7. Potential temperature (θ) of the bottom layer.

northward close to the Adelie Coast while the MCDW outside the shelf flows northwestward. The separation area between these water masses is characterized by strong velocity shears and meanders, which increases the turbulence and, in turn, can enhance resuspension phenomena, a point that will be discussed below.

The lack of current meter data for this area does not allow any direct estimation of absolute HSSW velocities, but Kurgansky *et al.* (2002) developed a novel method for inferring the absolute velocity field from the analysis of the temperature and salinity fields. It is a potential vorticity version of the classical β-theories, applied not to the marine water density but to salinity and temperature. The application of such a technique (Falcini and Kurgansky, 2005) suggests the identification of a very shallow (∼100 m deep) no-motion level, a choice supported by the flatness of the 100 m deep isopycnals in this working area. With this tentative identification, the classical Margules-Witte formula, as applied to the upper layers, implied that the northward HSSW flux was about ∼0.3–0.5 Sv.

5. First analysis of the sedimentary patterns

The light-transmission data and the samples from the Niskin bottles, giving water turbidity and Total Particulate Matter (TPM) concentration, respectively, were used to gain some systematic insight into the interaction of the sediments with the bottom water.

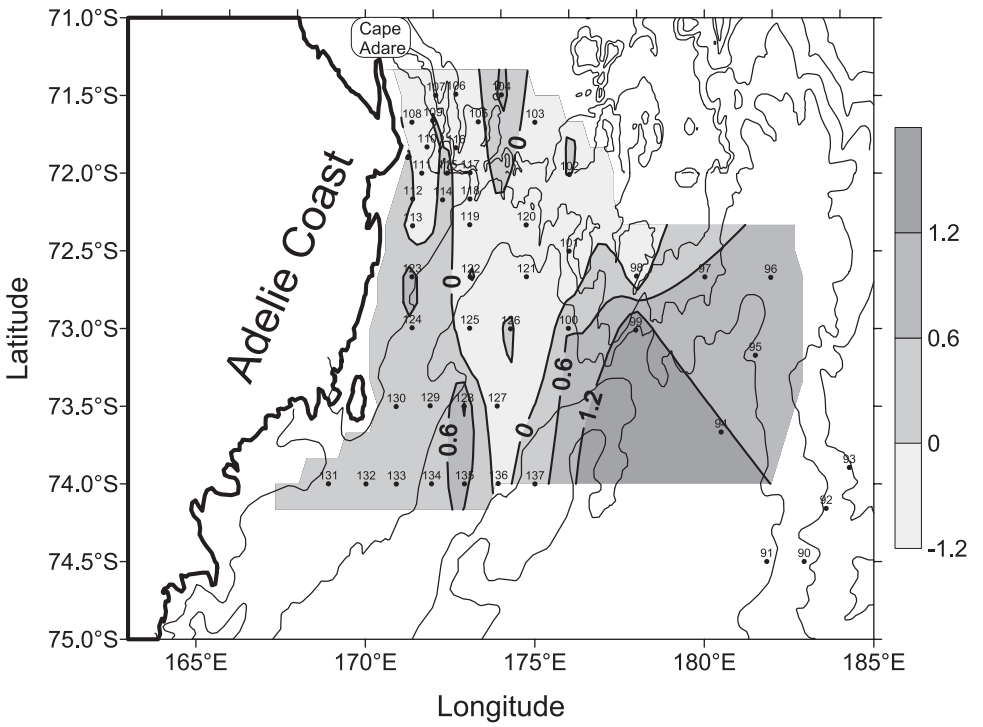

Figure 8. TPM $\Delta_{(B-I)}$ difference in mg l^{-1}, between the value of the concentration near the bottom (B) and in the intermediate layer (I).

Observed concentrations of TPM were in the range of 0.18 to 4.02 mg l^{-1} but some differences were found along the continental margin. In this section we focus our attention on the difference between the intermediate and the bottom layer (Δ_{B-I}) because the merely distributions of the TPM at the different depths do not add any relevant information; for that in the following we give only a short description of the TPM horizontal variability in the Ross Sea for both the surface and bottom layers without showing any map. In particular the horizontal distribution of the particulate matter appeared quite uniform over the shelf, between 1.10 mg l^{-1} (sea bottom) and 1.32 mg l^{-1} (surface). However, it also showed a rather strong vertical gradient at some locations near the Mawson Bank (stations 128 and 135). At the shelf break, where the CDW rises and interacts with the shelf waters (Figs. 2, 4 and 5), the observed particulate reached values greater than the average TPM in the adjacent stations (1.72 mg l^{-1} near the bottom and 2.03 mg l^{-1} in the surface water). Off the shelf break zone, at stations 104 and 105, the particulate near the bottom reached particularly high values, as much as 4.02 mg l^{-1}.

Of interest was also the systematic analysis of the Δ_{B-I} difference between the value of the TPM as observed 2-3 meters above the bottom and in the intermediate layer (Fig. 8). These intermediate waters were collected at depths between 200 and 400 m on the

continental shelf (MCDW), and also between 400 and 800 m over the continental rise (CDW). Many authors have studied the vertical distribution of particulate in density currents and a particularly clear representation for a homogeneous particulate is due to Stacey and Bowen (1988). However, in our case the bottom particulate was not really homogeneous and its vertical distribution could be different, as shown in detail in Figures 3, 9, 11, 12 and 13.

In synthesis, the difference between TPM data at the sea bottom and at intermediate depths (Δ_{B-I}) over the shelf ranged between 0 and 0.6 mg l^{-1}. It increases near the banks ($0.6 < \Delta_{B-I} < 1.0$ mg l^{-1}) probably due to tides, and off the shelf break it reached the highest values ($\Delta_{B-I} \approx 3$–4 mg l^{-1}) around deep station 105. In the shelf-break region the water had larger shears and was also rich in bottom particulate. Indeed we can exclude an increase in the bottom sediment concentration as due to CDW upwelling (as nicely discussed by Van Weering *et al.,* 2002) since this last effect mainly occurs at the stations in the inner shelf region. So, this comparison of the benthic water and the intermediate water concentration is most probably related to sediment re-suspension due to the benthic water-sediment interaction.

With regard to the light transmission information, the minimum in-beam transmission in the water column (between 70–80%) was naturally in the mixed surface layer. Here the water turbidity was essentially due to the rather homogenous presence of organic particulate matter, phytoplankton (revealed by fluorescence data) and also light debris from moraines and glacier melting. Immediately below the pycnocline, the light transmission increased to values ≈90 %. This situation was quite evident in all the sampling stations over the shelf, but near the shelf bottom the scenario could be different.

It is indeed of some interest how often a concomitant jump of light transmission, θ, (decrease) and salinity, S, (increase) is observed in these data, revealing a thin denser benthic layer, characterized by vertically homogeneous values for light transmission, θ, and S. Due to the particular shape assumed by the curves of the hydrographic and light transmission data, in this work we call such a homogenous layer a "tripod." This characteristic is most probably due to a thin turbulent current which is also mixed with some sediments, namely a density–turbidity current. An example of such benthic layers is shown in Figure 9 (station 125).

Such "tripods" are almost detectable over all the working area (Fig. 10). In the region of our main interest, namely where the bottom temperature is ∼−1.9°C, the benthic layer thickness is ∼10–50 m for stations in transects A, B and C. At station 120, which has the sharpest bottom slope, it reaches a thickness of ∼100 m, while further north it is thinner, around 10 m. However, it reaches a thickness of ∼ 50 m at the farthest stations of the slope. A more detailed analysis reveals: (i) casts showing a well mixed water column close to the bottom, characterized by a sharp increase in the turbidity of the benthic layer. As an example, at station 137, located on the inner shelf west of the Mawson Bank inside the Joides Basin (Fig. 11), a negative jump in the light transmission data near the sea-bottom is evident, with a difference of ∼4% in light transmission between the intermediate and the

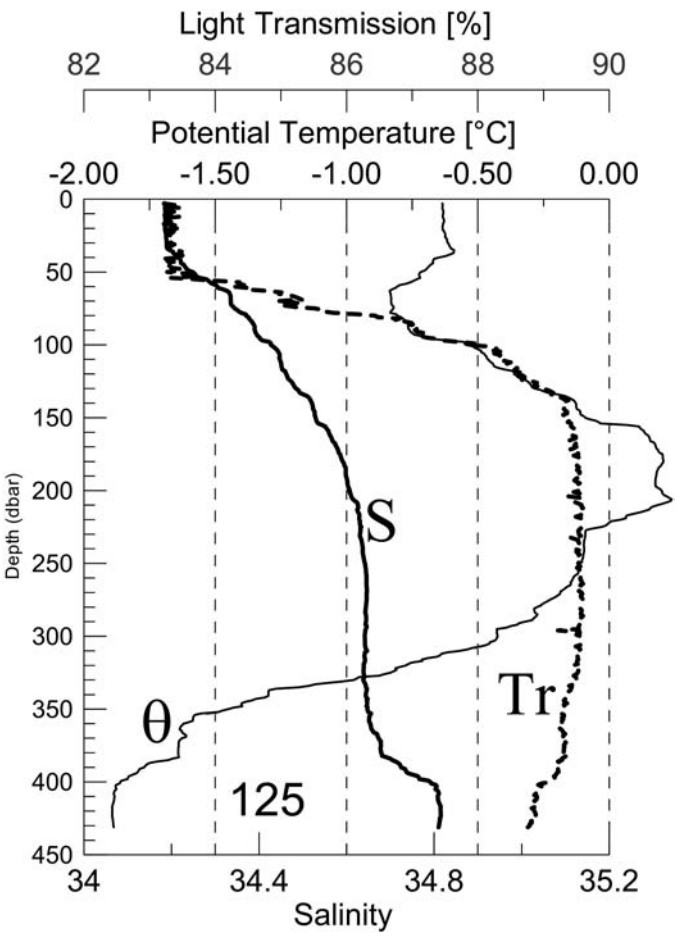

Figure 9. Potential temperature (θ), salinity (S), and light transmission (Tr) data versus depth for station 125, transect B.

lowest levels. (ii) casts showing a water column with distinct water masses in the intermediate and deep (benthic) layers. Most of these casts are located along the southern banks and reliefs. Indeed at stations 134, 135 and 136, located on the Mawson Bank, clear "tripod" structures are detectable (cast 135, shown in Fig. 3). We also noticed that at stations 134 and 135 the Δ_{B-I} difference in sediment concentration between the bottom and intermediate layers was rather mild, ranging between 0.6 and 1.0 mg l^{-1} (Fig. 8). This would seem to be the effect of tides or boundary mixing, as suggested by one referee. (iii) a similar behavior is also noticeable for some casts on the shelf: for example at stations 121, 122, and 123 (Fig. 5) the benthic layer is identified by a mild increase in water turbidity. In this case the Δ_{B-I} is positive at stations 122 and 123, but not at the more external station 121 (Fig. 8), which is also on the Mawson Bank and where the transmission values show

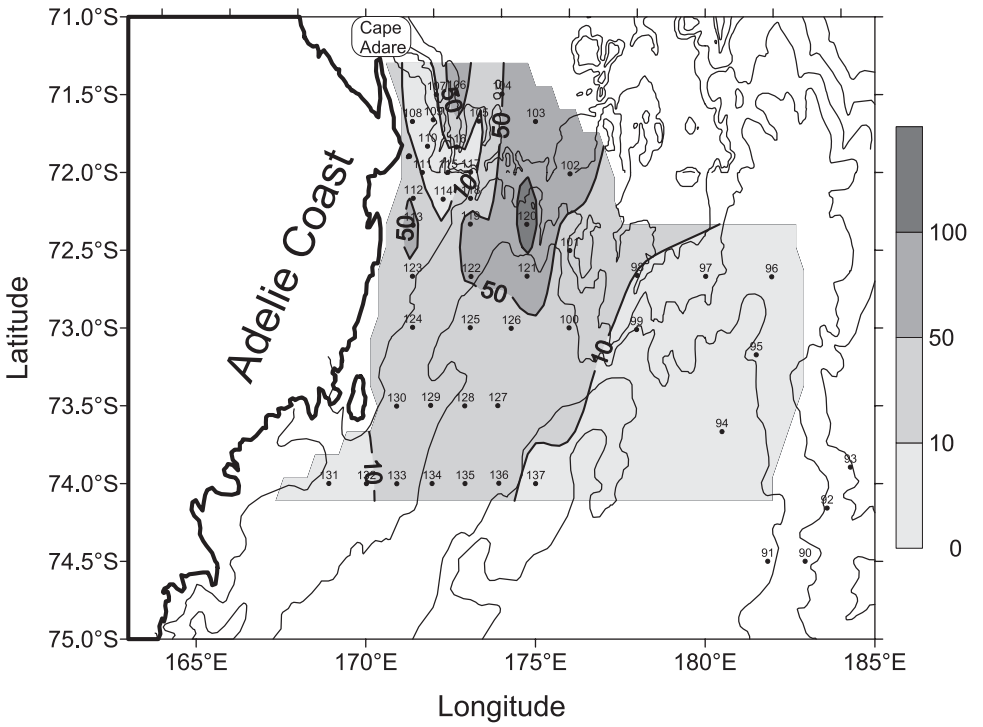

Figure 10. Thickness of the benthic layer on the sea bottom in meters; namely the distribution of the layer height where potential temperature, salinity, and turbidity changes contemporarily.

only a mild increase in turbidity (Fig. 12). (iv) finally, in the northernmost area—on the slope—the thermohaline field close to the bottom does not reveal the presence of HSSW. As shown in Figure 7, where the potential temperature in the lowest layer is analyzed, the stronger gradients are located close to stations 114, 115, 117, 118, 109, and 110. This confirms the hypothesis that in this area the dense water mixes and apparently disappears at the shelf break boundary, a region where the hydrographic casts performed during the 1994/95 survey were not close enough to detect the bottom currents, that could develop at small spatial scale and/or with a temporal intermittency.

It is also of interest that these northernmost stations are characterized by small benthic layer thicknesses (about 10 m only, shown in Fig. 10) and by a tongue (stations 114, 115, and 109) of rather high values of Δ_{B-I} (Fig. 8). In the deep basin (station 105, Fig. 13) the light transmission profile shows a smooth step-like structure. Moreover, the TPM values at these stations reveal a gradient between the deepest and intermediate layers ($0.6 < \Delta_{B-I} < 1.2$ mg l^{-1}), but the largest gradient ($0.6 < \Delta_{B-I} < 2.4$ mg l^{-1}) is observed at the deep station 105 (Fig. 8).

It is also possible to obtain an indirect estimate of the velocities of this turbulent benthic layer. Indeed we applied the results of Necker *et al.* (2002), who found that the onset of

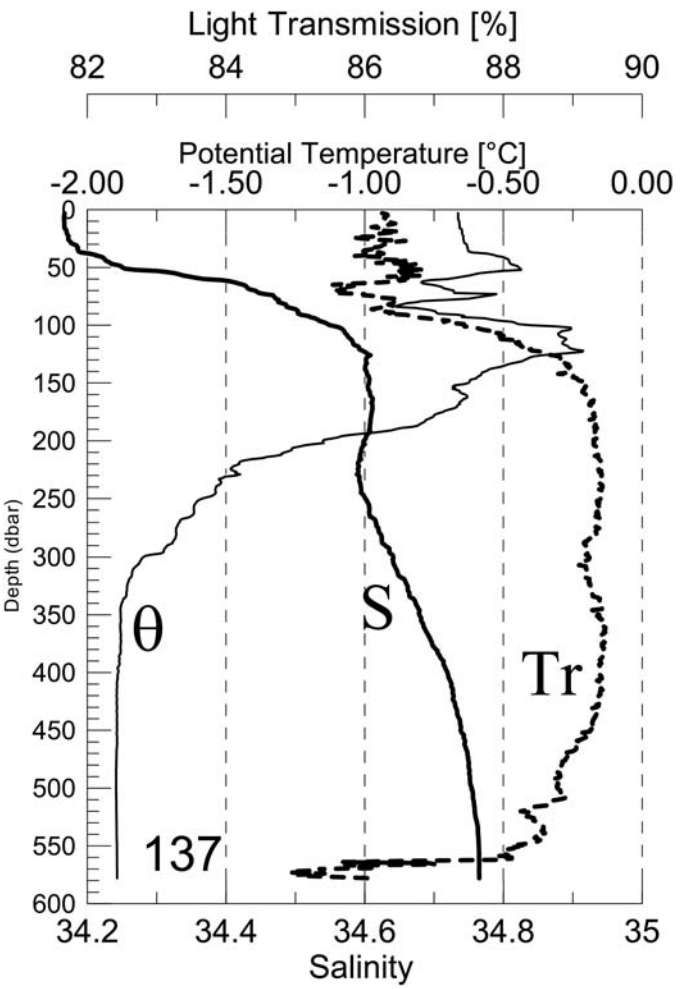

Figure 11. Potential temperature (θ), salinity (S), and light transmission (Tr) data versus depth for station 137, transect A.

sediment resuspension happens due to the wall shear stress $Y \sim \frac{\rho}{\Delta\rho}\frac{uv}{ghd} \sim 0.4$–$0.07$ (in nondimensional units). Here u is the unknown benthic water velocity, d is the sediment size ≈ 30 μm, h is the benthic layer thickness ≈ 30 m, ν is the water viscosity $\approx 10^{-2}$ m s^{-2} and $\Delta\rho/\rho \sim 2$ is the relative density difference between water and sediments. All this gives large u values in the range 0.2–1.0 m s^{-1}, which, however, are similar to those measured in this area by Gordon *et al.* (2004). Furthermore, the application of the classical theory of Parker (1986) gives a velocity of about 0.5 m s^{-1}.

Consequently, assuming a benthic layer speed of 0.5 m s^{-1} (halfway between the two previous estimations) a remarkable flux moving northward in the benthic layer of about 1.4

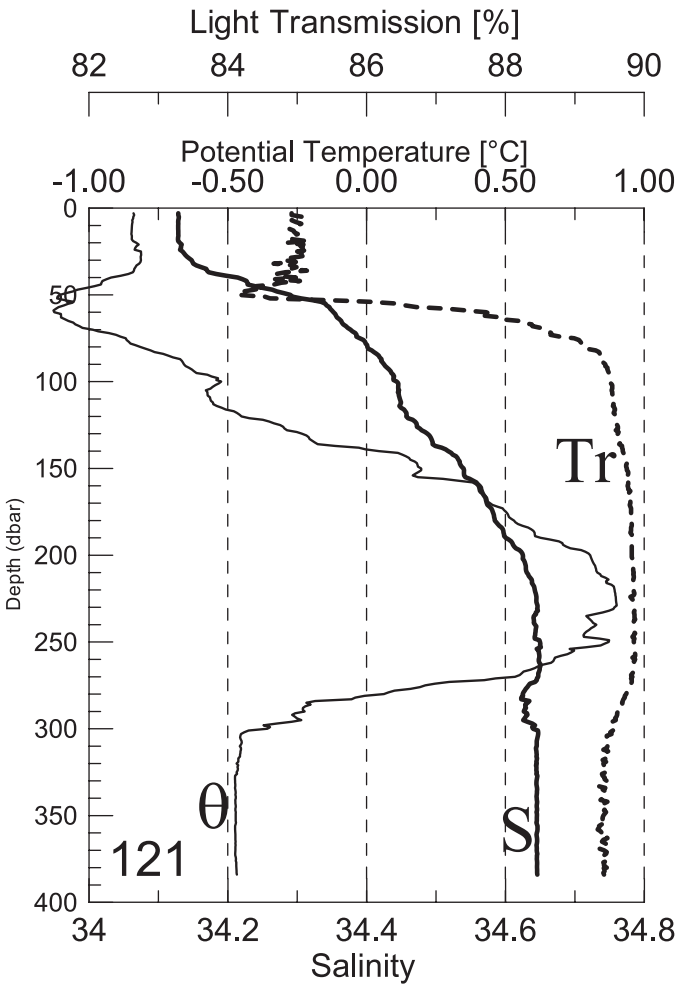

Figure 12. Potential temperature (θ), salinity (S), and light transmission (Tr) data versus depth for station 121, transect C.

Sv is estimated for transect A, while it is 0.8 Sv for transects B and C with rather large errors.

In synthesis, these data reveal the presence of a thin turbulent benthic current, correlated with a diffusion of sediments in the benthic layer. This is evident in all the sections of the shelf but its effect is more obvious at the northern stations, where the dense waters are mixed with bottom particulate (Huthnance *et al.,* 2002). The northward flux of the HSSW is 0.8, 0.4 and 0.5 Sv for transects A, B, and C respectively while the associated energetic benthic fluxes are larger: 1.40 Sv for transect A ad 0.8 Sv for transects B and C. Consequently the total flux of both HSSW and benthic water finally is 2.1 for transect A, 1.2 Sv for transect B and finally 1.1 Sv for transect C.

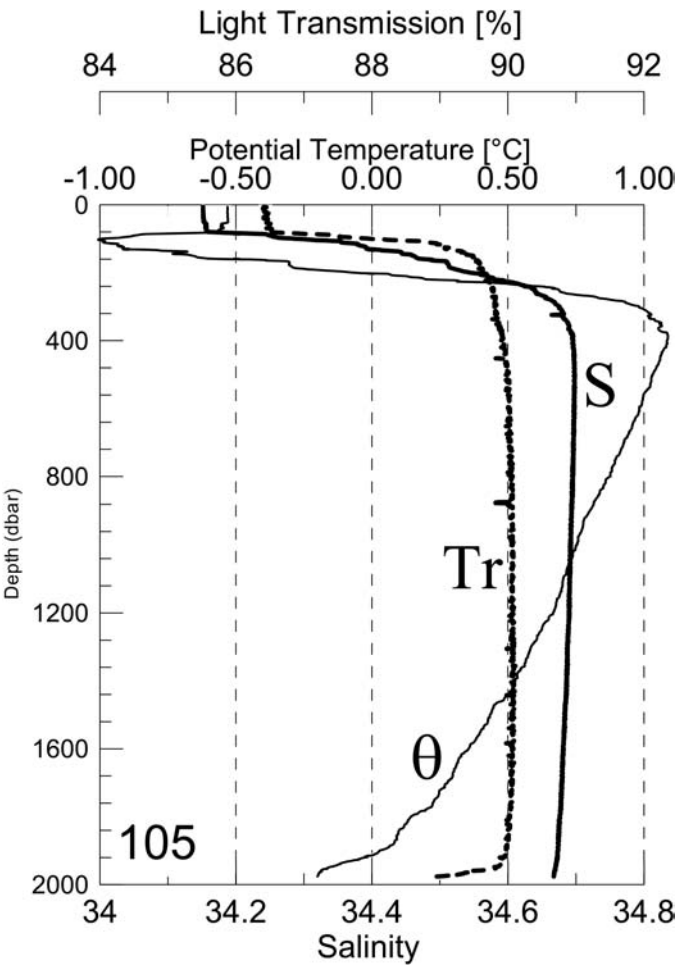

Figure 13. Potential temperature (θ), salinity (S), and light transmission (Tr) data versus depth for station 105, north of transect D.

As stressed by one referee, some aspects of this benthic layer will require some clarification. Its hydrologic origin, its dynamic relation with the slower upper HSSW layer, the effect on both layers of the Ekman benthic boundary, the possibility that this bottom HSSW current might be drained by the benthic energetic current, are open interesting questions, that need further investigations with appropriate experimental surveys.

6. Geostrophic and ageostrophic evolution of steady density currents

The preceding discussion suggests that it would be worthwhile to investigate the dynamics of a bottom current flowing steadily along the seafloor, driven by density

difference $\Delta\sigma \sim 0.1$ due to S $\sim$ 34.70 and very low $\theta \sim -1.9$°C. The presence of particulate matter of 1–4 mg l^{-1} should also be taken into account although this would only change the sample density by $1\text{–}4 \times 10^{-6}$ kg m^{-3}, as remarked by one referee. This certainly is not a main forcing but in this region, down-flows can reach 1.0 and 1.6 m s^{-1}, as observed in year 2003 by Gordon *et al.* (2004), and such velocities are probably indicative of turbidity effects.

Bottom flows are usually investigated using stream-tube models (Smith, 1975; Emms, 1997; Baringer and Price, 1997; Killworth, 2001) that deal with the bulk properties of the bottom current. Such models are successful in explaining the evolution of dense water outflows. In particular they identify two distinct phases in the evolution of a bottom current at the shelf break. The first is a rapid adjustment to a geostrophic state, marked by the vigorous entrainment of ambient water that lasts for approximately a few deformation radii. It is this entrainment that can explain why the dense water observed at station 111 of transect D has a temperature between that of HSSW ($\sim$80%) and MCDW ($\sim$20%).

The second phase is a rather slow descent along the shelf break (as suggested by the bottom temperature shown in Fig. 7), due to frictional decay (Killworth, 2001). Indeed, for small Rossby numbers there are three main components to the overall force balance. Two of these would occur under any model assumption: Coriolis force, orthogonal to the velocity and so oriented upslope, and gravity, oriented downslope. The third is the bottom drag, which in a slab-like flow can only appear as a body force $\approx -C\, u^2/h$. Killworth (2001) analyzed this kind of descent, also assuming a local equilibrium for the current thickness, all this, in practice, appearing as characterized by a rather constant Froude number. This implies that, under these hypotheses, the descent current path is mainly due to the sea bottom topography, and is more or less independent of the physics of the outflow.

It must be take into due account that these flows are not particularly stable. Therefore, intermittent structure characteristics of such instabilities could also be found in these outflows, as the "quick duration pulse" of Gordon *et al.* (2004). On the other hand Shapiro *et al.* (2003) discuss a tentative criterion to check the possibility of an accelerating breakdown (i.e. stable solutions do not exist) of these bottom currents, namely that $R_H = \Delta\rho \dfrac{g}{\rho f^2 L} s > 1$. Here s is the bottom slope, g is the gravity, f is the Coriols parameter, $\Delta\rho/L$ is the cross-slope density gradient. In our case R_H is slightly smaller than 1. This gives some support to the idea that the density gradient is not strong enough to trigger cascading, finally giving a rather stable descending current.

However, it should be remembered that besides entrainment and bottom friction, there are other important effects that are not considered in a slab model, such as an offshore-oriented marine canyon, eddy formation, Ekman benthic drainage or current-bottom particulate interaction that can affect the descent of the dense water, that are not considered in a slab model. In our case, however, detailed analyses of the bottom topography do not give any evidence of the presence of a submarine canyon (Davey and Jacobs, 2005). From the classical analysis of the energetic benthic current by Baines and Condie (1998), for h

larger than the Ekman frictional boundary layer thickness, namely $h > \sqrt{2\nu/f}$ where ν is the turbulent eddy viscosity, the down-slope flow can break up into a periodic set of eddies. These are due to vortex stretching of the entire water column; due to the down-slope motion of the water column and to Ekman drainage from the lowest layer.

But if $h < \sqrt{2\nu/f}$, it is the down-slope Ekman pumping that mainly influences the a-geostrophic current dynamics. Moreover, it can be shown (Wahlin, 2004) that along-slope bottom corrugations can channel dense waters downward. In the Appendix we show how a similar effect can be caused by pressures due to an upper layer moving westward, as is the case in the Ross Sea. So for $h < \sqrt{2\nu/f}$, eddies cannot form and a thin viscously-controlled layer extends down over the shelf break, to its density level or to a level where it is eroded by turbulent mixing. Its velocity scale is larger than $u \sim \frac{g'}{f}\frac{dh}{dy} \sim 0.2$ m s^{-1} (Baines and Condie, 1998), if the sediments do not affect this down-flow.

In this way it is possible to obtain a large rather slow bottom current descending as a classical stream-tube (Killworth, 2001) as probably seen in our station 111. It is also possible to see a vigorous thin viscosity-controlled benthic layer (perhaps with a small quantity of sediments), flowing down-slope as seen in our deep stations 104 and 105. It is also possible that all this can evolve into a classical impulsive turbidity current, such as the short pulse observed by Gordon *et al.* (2004), if a large enough quantity of bottom particulate is present. However, it is also possible to hypothesize that for a small amount of available bottom particulate, in a sort of equilibrium, a different, slowly-evolving density-turbidity current can finally emerge, as suggested by the large Δ_{B-I} (0.6 ÷ 2.4 mg l^{-1}) particulate gradient near the bottom and by particularly high values for bottom particulate, up to 4.02 mg l^{-1}, at the northernmost stations.

7. Conclusions

In conclusion, the Cape Adare area studied in this paper presents some interesting physical characteristics, such as the northward flow of dense cold water, the presence of nepheloid structures and finally the "disappearance" of the observed bottom waters at the northern shelf break (Fig. 14). Therefore, the data shown here, as well as the results by Budillon *et al.* (1999, 2000, 2002), point to typical features of the evolution of the dense shelf waters in the Ross Sea. This bottom shelf water, namely HSSW, flows geostrophically until some perturbation occurs, which most probably consists of the interaction with the CDW along the Antarctic Slope Front (Figs. 4, 7, and 8). But while north of transect D the presence of the cold waters is no longer fully detectable (Figs. 6 and 7) probably due to the sampling resolution of an intermitting phenomenon, some traces remain in the nepheloid layers and sedimentary structures observed off the shelf break.

Intermittent structures characteristic of such instabilities have been observed in the HSSW outflow as the "short duration pulses" found by Gordon *et al.* (2004). This suggests that the detection of such structures in the outflow of HSSW from the Ross Sea would

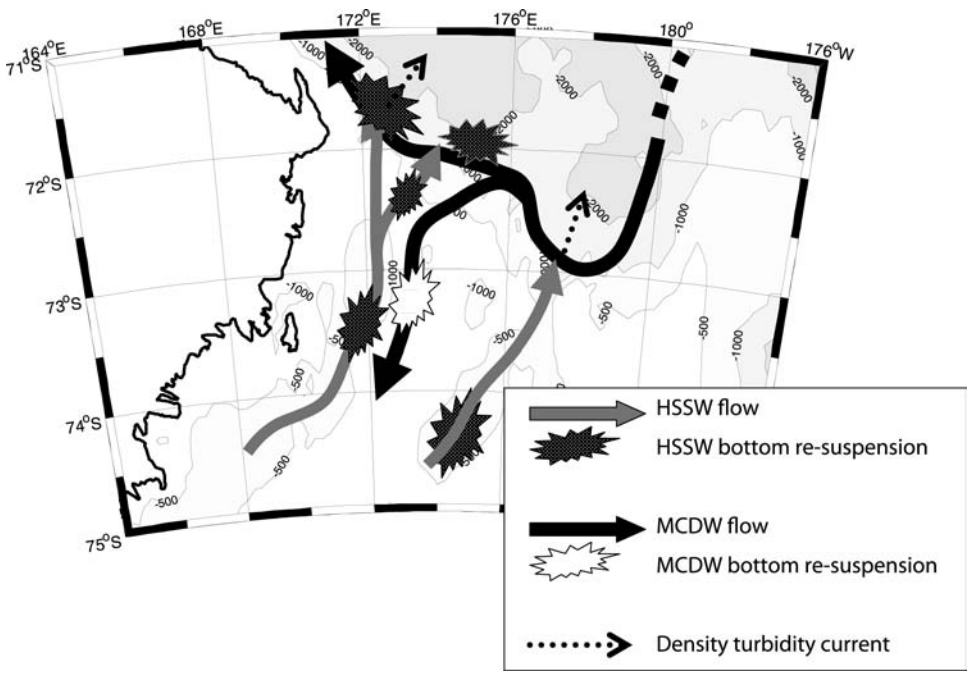

Figure 14. Schematic reconstruction of the most relevant interactions with the bottom sediments on the shelf.

require specific investigations with either the simultaneous deployment of a series of moorings and/or to measure repeated casts located in the nominal outflow, to reconstruct a hydrological time-series. Due to the inadequate sampling strategy, in both time and spatial scales, this study cannot resolve these questions, but it stresses the relevance of bottom current instabilities in the export of dense waters from the Ross Sea shelf to the open Ocean.

In more detail, during its northward flow the dense HSSW mixes with CDW and partially descends as a stream-tube (Killworth, 2001), as probably seen in station 111. The estimated HSSW fluxes range from 0.8 Sv south of Couleman Island to 0.5 Sv toward the shelf break. But over the shelf one can also see "tripods," namely hydrologic structures due to a thin vigorous benthic current, mixed with bottom sediments, moving northward. We can see that the "tripod" thicknesses over the shelf increase toward the N-N-E (Fig. 10). The estimated fluxes of such flows moving close to the bottom are larger in the southern part (1.4 Sv) and they decrease close to the shelf break (0.8 Sv). North of the Antarctic Slope Front these cold waters mix, sink and finally disappear while in some locations further north particularly large Δ_{B-I} sediment differences are present (stations 104 and 105, Fig. 8) and it is here that the highest TPM concentration is found.

This suggests that these dense waters have a regular geostrophic flow south of the

Antarctic Slope Front. This equilibrium is presumably destroyed by the interaction with the CDW, but there must also be some influence from bottom sediment erosion. This has been observed in the northernmost working area where Figures 7, 8 and 10 show how a strong horizontal temperature gradient, indicative of bottom water down-flow, and a rather large quantity of sediments have been observed in the same small area. In the northwestern Ross Sea the shelf is bordered by important steep faults caused by disjunctive tectonic activity in the substratum; the overall result is an abrupt continental slope where the down-flow of benthic currents, mixed with sediments, occurs. Reaching the bottom at the end of the continental slope such currents contribute to the formation of a significant bottom nepheloid layer, as detected in stations 104 and 105 at a depth of ~2000 m (and a similar mechanism probably occurs at stations 99 and 100 also).

In such a complex situation, further observation could certainly be of considerable value.

Acknowledgments. We would like to thank Dr. F. Falcini and Professor M. Kurgansky for furnishing us with information on their investigation into mass and heat fluxes in the Ross Sea. We would also like to thank Dr. M. Capello for his expert technical help and Dr. D. Prosperi for help and encouragement in the early stages of this research. The constructive comments and suggestions of the anonymous referees greatly improved the manuscript. This study was carried out as part of the Italian National Program for Research in Antarctica (CLIMA project) and was financially supported by ENEA through a joint research program.

APPENDIX

We now analyze pressure values in a (x, y) plane with y toward North and x toward East. We consider a layered Ocean for $y < 0$, *with a straight coastline at* $y = 0$, but with a gulf in a southern region where $y < 0$. The sea bottom b in the gulf is assumed flat, with constant $b = b_0$. Off the gulf the sea bottom slopes to larger depths as $b = b_0 + F(y) \sim b_0 + By$.

Off the gulf there is a westward surface current with velocity $V \sim$ constant, while inside the gulf the upper layer is assumed to be motionless. Calling now h_1 the air-sea elevation and $H(x, y, z) = H_2 + h_2\,(x, y, t)$ the interface between layers, we have in the upper layer $p_1 = p_o + g\,\rho_1\,(h_1 - z)$ where g is the gravity, the upper layer density is ρ_1. Assuming densities and velocities rather homogeneous inside each layer, in the Ocean the air-sea surface slope is approximately uniform. Consequently, the geostrophic balance (Gill, 1977) gives $fV = -g\dfrac{\partial h_1}{\partial y} \approx$ constant and $g\dfrac{\partial h_1}{\partial x} \sim 0$, where f is the Coriolis parameter. The same holds inside the gulf, but since $V = 0$ there the air-sea surface is flat.

In the Ocean second layer one has

$$p_2 = p'_o + g\rho_2(h_2 - z) + g\rho_1(h_1 - h_2) = p_o + g\rho_1 h_1 + g(\rho_2 - \rho_1)h_2 - g\rho_2 z \qquad \text{(A1)}$$

with p_o, p'_o, constants, And so we have

$$-\frac{1}{\rho_2}\frac{\partial p_2}{\partial x} = -g\left(\frac{\rho_2 - \rho_1}{\rho_2}\right)\frac{\partial h_2}{\partial x} - g\frac{\rho_1}{\rho_2}\frac{\partial h_1}{\partial x} = -\left(\frac{\rho_2 - \rho_1}{\rho_2}\right)g\frac{\partial h_2}{\partial x} \tag{A2}$$

$$-\frac{1}{\rho_2}\frac{\partial p_2}{\partial y} = -\frac{\partial h_2}{\partial y}g\left(\frac{\rho_2 - \rho_1}{\rho_2}\right) - g\frac{\rho_1}{\rho_2}\frac{\partial h_1}{\partial y} = -g\frac{\rho_2 - \rho_1}{\rho_2}\frac{\partial h_2}{\partial y}$$
$$+\frac{\rho_1}{\rho_2}fV \cong -\frac{\partial h_2}{\partial y}g\left(\frac{\rho_2 - \rho_1}{\rho_2}\right) + fV \tag{A3}$$

namely a forcing fV, towards offshore, is the overall effect in the Oceanic lower layer of the surface current flowing westward. And assuming $fV \sim 2 \times 10^{-5}$ m s^{-2} and $g' \sim 10^{-3}$ m s^{-2} and slopes of $\sim 10^{-2}$, this looks comparable with the interface pressure gradient.

REFERENCES

Baines, P. G. and S. Condie. 1998. Observations and modeling of Antarctic downslope flows: A review, *in* Ocean, Ice and Atmosphere: Interaction on the Antarctic Continental Margin, S. Jacobs and R. Weiss, eds., American Geophysical Union, *75,* 29–49.

Baringer, M. and J. Price. 1997. Momentum and energy balance of the Mediterranean outflow. J. Phys. Oceanogr., *27,* 1678–1692.

Bergamasco, A., V. Defendi and R. Meloni. 2002. Some dynamics of water outflow from beneath the Ross Ice Shelf during 1995–1996. Antarctic Sci., *14,* 74–82.

Budillon, G., G. Fusco and G. Spezie. 2000. A study of the heat fluxes in the Ross Sea Antarctica. Antarctic Sci., *12,* 243–254.

Budillon, G., S. Gremes Cordero and E. Salusti. 2002. On the dense water spreading off the Ross Sea shelf Southern Ocean. J. Mar. Sys., *35,* 207–227.

Budillon, G., M. Pacciaroni, S. Cozzi, P. Rivaro, G. Catalano, C. Ianni and C. Cantoni. 2003. An optimum Multiparameter mixing analysis of the shelf waters in the Ross Sea. Antarctic Sci., *15,* 105–118.

Budillon, G., S. Tucci, A. Artegiani and G. Spezie. 1999. Water masses and suspended matter characteristics of the western Ross Sea, *in* Ross Sea Ecology, F. M. Faranda, L. Guglielmo and A. Ianora, eds., Springer-Verlag, 63–81.

Davey, F. J. and S. S. Jacobs. 2005. The morphology of the Ross Sea shelf and northwest margin, *in* 3rd International Conference on the Oceanography of the Ross Sea Antarctica, Venice, 10–14 October 2005.

Emms, P. 1997. Streamtube models of gravity currents in the ocean. Deep-Sea Res., *44,* 1575–1610.

Falcini, F. and M. Kurgansky, 2005. Outflow of cold dense water off the Ross Sea Antarctica. Preprint—Phys. Dept. University La Sapienza, Rome.

Gill, A. E. 1977. The hydraulics of rotating–channel flow. J. Fluid Mech., *80,* 641–671.

Gordon, A. L. 1967. Structure of Antarctic waters between 20°W and 170°W: Antarctic Map Folio Series V, *6,* 1–10.

Gordon, A. L. and P. Tchernia. 1972. Waters of the continental margin off Adelie coast, Antarctica, *in* Antarctic Oceanology II: The Australian—New Zealand Sector, D. E. Hayes, ed., American Geophysical Union, 56–69.

Gordon, A. L., E. Zambianchi, A. Orsi, M. C. Visbeck, F. Giulivi, T. Whitworth III and G. Spezie. 2004. Energetic plumes over the western Ross Sea continental slope. Geophys. Res. Lett., *31,* L21302, doi:10.1029/2004GL020785.

Hogg, A. J., M. Hungarish and H. E Huppert. 2000. Particle driven gravity currents: asymptotic and box model solutions. Eur. Jour. Mech., B, *19,* 139–165.

Huthnance, J. M., H. M. Van Aken, M. White, E. D. Barton, E. F. Le Cann, E. F. Coelho, E. A. Fanjul, P. Miller and J. Vitorino. 2002. Ocean margin exchange—water flux estimates. J. Mar. Sys., *32,* 107–137

Jacobs, S. S. 1991. On the nature and significance of the Antarctic Slope Front. Mar. Chem., *35,* 9–24.

Jacobs, S. S., A. F. Amos and P. M. Bruchhausen. 1970. Ross Sea oceanography and Antarctic Bottom Water formation. Deep-Sea Res., *17,* 935–962.

Jacobs, S. S. and J. C. Comiso. 1989. Sea ice and oceanic processes on the Ross Sea continental shelf. J. Geophys. Res., *94,* 18195–18211.

Jacobs, S. S., R. G. Fairbanks and Y. Horibe. 1985. Origin and evolution of water masses near the Antarctic continental margin: evidence from $H_2^{18}O/H_2\ ^{16}O$ ratios in seawater, *in* Oceanology of the Antarctic Continental Shelf, S. S. Jacobs, ed., American Geophysical Union, *43,* 59–85.

Killworth, P. 1983. Deep convection in the world Ocean. Geophys. Space Phy., *21,* 1–26.

——2001. On the rate of descent of overflows. J. Geophys. Res., *106,* 22267–22275.

Kurgansky, M. V., G. Budillon and E. Salusti. 2002. Tracers and potential vorticities in ocean dynamics. J. Phys. Oceanogr., *32,* 3562–3577.

Locarnini, R. A. 1994. Water Masses and Circulation in the Ross Gyre and Environs. PhD dissertation, Texas A&M University, 87 pp.

Necker, F., C. Hartel, L. Kleiser and E. Meiburg. 2002. High-resolution simulations of particle driven density currents. Int. Jour. Multiphase Flow, *28,* 279–300.

Parker, G., Y. Fukushima and H. M. Pantin. 1986. Self accelerating turbidity currents. J. Fluid Mech., *171,* 145–181.

Piccazzo, M. and S. Tucci. 1983. Distribuzione e trasporto di materiale particolato sospeso nei canyons di Genova. Atti V Congresso AIOL (in Italian), Stresa, 675–690.

Pierce, J. W., S. Tucci and G. Fierro. 1981. Assessing variation in suspensates, Ligurian Sea northwestern Mediterranean. Geo-Mar. Lett., *1,* 149–154.

Rodman, M. and A. Gordon. 1982. Southern Ocean bottom waters in the Australia—New Zealand sector. J. Geophys. Res., *87,* 5771–5778.

Quadfasel, D., H. Kudrass and A. Frische. 1990. Deep-water renewal by turbidity currents in the Sulu Sea. Nature, *348,* 320–322.

Shapiro, G. I., J. M. Huthnance and V. V. Ivanov. 2003. Dense water cascading off the continental shelf. J. Geophys. Res., *108, C12,* 3390, doi:10.1029/2002JC001610.

Smith, P. C. 1975. A stream-tube model for bottom boundary currents in the ocean. Deep-Sea Res., *22,* 853–873.

Stacey, M. W. and J. A. Bowen. 1988. The vertical structure of turbidity currents and a necessary condition for self-maintenance, J. Geophys. Res., *93,* 3543–3553.

Trumbore, S. E., S. S. Jacobs and W. M. Smethie Jr. 1991. Chlorofluorocarbon evidence for rapid ventilation of the Ross Sea. Deep-Sea Res., *38,* 845–870.

UNESCO. 1983. The acquisition, calibration and analysis of CTD data. A report of SCOR WG 51. Technical Papers in Marine Science, 54–59.

——1988. Algorithms for computation of fundamental properties of seawater. Technical Papers in Marine Science, 44–53.

Van Weering, T. C. E, H. C. de Stigter, W. Boer and H. de Haas. 2002. Recent sediment transport and accumulation on the western Iberian Margin. Prog. Oceanogr., *52,* 349–372.

Wahlin, A. K. 2004. Downward channeling of dense water in topographic corrugations. Deep-Sea Res., *51,* 577–590.

Wahlin, A. K and G. Walin. 2001. Downward migration of dense bottom currents. Environmental Fluid Mech., *201,* 257–279.

Received: *13 May, 2004;* revised: *16 May, 2006.*